Effects of the Inclusion of the Spin Label 10-Doxyl-Stearic Acid on the Structure and Dynamics of Model Bilayers in Water: Stearic Acid and Stearic Acid/Cholesterol (50:20)

Alberto S. Garay[†] and Daniel E. Rodrigues*[,†,‡]

Departamento de Física, Facultad de Bioquímica y Ciencias Biológicas, Universidad Nacional del Litoral, and INTEC (U.N.L.−CONICET), C.C. 242, Ciudad Universitaria, C.P. S3000ZAA, Santa Fe, Argentina

Received: May 4, 2007; In Final Form: November 9, 2007

The effects of the insertion of a spin-labeled molecule (10-doxyl-stearic acid) on the structure and dynamics of model lipid bilayers in gel-like as well as in liquid-ordered-like phases are studied using molecular dynamic simulations. The perturbing effects of the labeled molecule on the structure of the bilayers are analyzed. We have also studied the relationship between the structural and dynamic properties of the bilayer phase and those of the labeled molecule. We found that the insertion of the labeled molecule in the bilayer at the concentration considered here (1:70) produces local and global perturbations in the gel-like phase. There is an increase of the area associated with the lipid molecules that produces a larger tilting angle of this condensed phase. In this gel-like phase, we also found that the *z* component of the order parameter of the labeled molecule associated with the electron paramagnetic resonance (EPR) spectra has the same temperature dependence as the axial correlation times of the lipid molecules. The mechanism by which the doxyl reorientation senses the dynamics of the layers is determined by the correlation between the gauche defect transitions of the labeled alkyl chain and its environment. For the liquid-ordered-like phase, we found that cholesterol molecules play the role of wedges that open free spaces in the lipid structure below the ring position and order the alkyl chains at the depths of the rings, leading to small inclination angles. The doxyl ring of the labeled molecule is located just below the cholesterol ring moiety, having fewer gauche defects than in the case of the gel-like phase. The change in depth of the doxyl ring causes a reorientation of this group that leads to an increase of the order parameter as the temperature rises.

Introduction

Electron paramagnetic resonance (EPR) spectroscopy in spin-labeled molecules has been successfully applied to the study of the dynamics and structure of doped biomembranes for more than 20 years. Relevant information has been obtained with this technique in lipid bilayers, for example, dipalmitoylphosphatidylcholine (DPPC)/water model,[1,2] fatty acid films,[3−5] and biological membranes.[6−9] The advantage of EPR spectroscopy is based on its high sensitivity which makes it especially suitable for the study of interfacial phenomena as compared with other techniques like nuclear magnetic resonance. EPR requires the presence of paramagnetic centers that can be provided by doping the sample with spin-labeled molecules unless the native system has unpaired spins. The order parameter *S* of the spin-labeled molecule can be estimated, since the EPR spectral features derived from the hyperfine splitting are directly related to the dynamics of its molecular orientation.[2] The EPR spectral response is the result of two combined effects: (a) the distribution of values of the spin orbital orientation relative to the magnetic field, and therefore the orientation of the labeled molecular group, and (b) the motion dynamics of this group. We will refer to the former factor as the "orientational" contribution, which will be a central issue in this work. The second factor leads to an averaging effect of the hyperfine derived spectral features when the motion is fast enough and will not be considered here. The narrowing of each of the hyperfine components is heuristically associated with a faster dynamics of the labeled molecule and used to quantify this property. It is usually assumed that the dynamics of the spin-labeled molecule carries out information about its environment, although a detailed comparison of the dynamics of this molecule and its individual environment at the molecular level is lacking. Some differences between the dynamics of the spin-labeled molecule and that of lipids when they are in solution have been pointed out by Hakansson et al.[10] Wisniewska et al.[11] also found that the gel−liquid crystalline (LC) phase transition temperature of DPPC measured by EPR using a labeled stearic acid (SA*) probe changes depending on the doping. Since a better understanding of the structure and dynamics of lipid bilayers has been achieved in the past decade,[12−15] it has become more relevant to establish how the EPR of spin-labeled molecules senses and perturbs their environment.

Molecular dynamics (MD) is a useful tool to study these effects, since it can provide atomic scale detailed information about the behavior of the layer and the spin-labeled molecule. As our model system for this study, we have chosen a simple stearic acid (SA) bilayer (system A) and a mixed stearic acid/cholesterol bilayer (system B) in water. The former is assumed to represent a lipid bilayer in the gel-like phase, while the second corresponds to the liquid-ordered-like phase. Multilayers of pure SA have been well characterized experimentally in Langmuir−Blodgett films and show a regular arrangement of the fatty acid molecules.[16,17] SA is the lipid carrier of some of the most popular spin labels used to characterize lipid membranes.

* Corresponding author. E-mail: daniel.rodrigues@dfbioq.unl.edu.ar. Phone/Fax: +54 (342) 4575-213.
[†] Universidad Nacional del Litoral.
[‡] INTEC (U.N.L.−CONICET).

10.1021/jp0734171 CCC: $40.75 © 2008 American Chemical Society
Published on Web 01/17/2008

Therefore, the comparison of the variables associated with the environment and the marker are straightforward. Despite its simplicity, the SA molecule is an amphiphile with a small polar head and a long alkyl hydrophobic chain. Nevertheless, it has a polar head much smaller than that of phospholipids, which leads to important differences in the phase diagram of their bilayers.

SA layers are relevant on their own, since the stratum corneum of the skin, the outermost layer of the epidermis, is composed of stacked fatty acid layers.[18,19] Experimentally, it is also known that SA forms Langmuir−Blodgett films, which have attracted considerable interest over the past years[20,21] in connection with highly specific sensors or devices based on molecular electronics.

As the spin-labeled molecule, we used a SA with the doxyl ring (nitroxide 2-doxylpropane (4,4′-dimethyloxazolidine-*N*-oxyl)) at position 10 (SA*). Although the most used doxyl-labeled SA molecules are those with rings at positions 5, 12, and 16, we chose to study the one labeled at position 10, as this roughly corresponds to the geometrical center of the layer. However, the conclusions at which we arrived should also be applicable to the 12-doxyl-SA.

The arrangement and dynamics of the spin-labeled molecule in a compact system like gel phase self-assembled lipid layers have been the subject of many qualitative analyses. Wisniewska et al.[11] have measured the gel−LC transition temperature in DPPC samples doped with 5-, 9-, 12- and 16-doxyl-labeled SA by EPR spectroscopy and in nonlabeled samples using calorimetric measurements. They found that the labeled DPPC samples have a lower gel−LC transition temperature as determined by EPR than that obtained from differential scanning calorimetry. The largest disagreement appears when samples are labeled with the 9-doxyl-SA. It has also been suggested that in ordered phases the labeled molecules could be segregated.[22] Risse et al. have studied SA Langmuir−Blodgett films of labeled and nonlabeled samples using near edge X-ray absorption fine structure (NEXAFS) and EPR spectroscopy.[3,4] They found that the presence of the doxyl-labeled molecules alters the structure and dynamics of the layers, although they were not able to precisely determine the label concentration in the samples. They found inconsistencies in the interpretation of the NEXAFS results for labeled layers that were concealed using qualitative arguments about the dynamics of the spin-labeled molecule. They conclude that the motion of the labeled molecule is a cooperative effect with its surrounding and suggest an induced increase of the area per lipid.

Conversely, it is well-established that the liquid crystalline (LC) phase of phospholipids is probably the most relevant for studies related to its biological function in membranes. Consequently, it is important to extend the above-mentioned studies to a lipid layer having as many as possible common features as those observed in LC phospholipid phases. The incorporation of cholesterol into phospholipid bilayers leads to the formation of a new phase, the liquid-ordered one. Although the existence as a thermodynamic isolated phase and its diagram boundaries have been questioned, it is assumed that the liquid-ordered phase shares many common features with the LC phase, having, however, lower conformational disorder in the alkyl chains.[23,24] It has often been argued that the disorder of these phases is strong enough to preclude the perturbation effects caused by the labeled molecule, although as has already been revealed experimentally[22] and will be shown below this is not completely true.

We performed MD simulations of the systems under consideration to obtain a detailed atomic scale description of the properties of the labeled molecule and nonlabeled lipid layers. The aim of this work is (a) to correlate the changes of the bilayer properties with those surveyed by the spin-labeled molecule and (b) to understand how the presence of this kind of molecule perturbs the bilayer behavior.

In this paper, we analyze four systems at several temperatures: model A, pure SA bilayer in water; model A*, pure SA bilayer labeled with one SA* molecule per layer in water; model B, a bilayer composed of a mixture of SA and cholesterol in a 50:20 molar ratio in water; model B*, the previous model B labeled with one SA* molecule per layer in water. Models A and B (without SA*) were used to get some structural and dynamic properties of the systems without the perturbation introduced by the labeled molecules. For pure SA layers (model A), there is experimental information from the lateral pressure−area isotherms in monolayers and X-ray diffraction of Langmuir−Blodgett (LB) films.[16,17,21,25] These results allow us to check the consistency of the parametrization used in the force field of the MD simulations to reproduce the experimental information. Model B has been used previously as a lipid model for the stratum corneum.[19]

The thermal effects over the lipid bilayer and the labeled lipid were studied by simulating each model at four different temperatures (285, 300, 315, and 330 K). This range was chosen because it is near the conditions used in the experimental setups.

In this work, we analyze several structural and dynamic features of the SA* and its molecular environment. In forthcoming papers, we will discuss the simulated EPR spectra calculated from the trajectory of the spin label along the simulation and the effects of labeling the SA at different positions. Similar works on phospholipid bilayers are in progress.

We analyze the following properties for each system to characterize the results of the MD simulations: (i) the average structure factor that brings information about the two-dimensional long range order, (ii) the average fraction of alkyl dihedral angles in the trans conformation to account for the number of gauche defects in the SA alkyl chain, (iii) the average inclination and azimuthal angles of the SA long axis to survey the tilting of the molecules, (iv) the average molecular area associated with each species, (v) the average order parameter tensor profiles that contribute information about the orientation of the segments of the alkyl chains and their motion, and finally (vi) the average angular autocorrelation functions and the correlation times for the axial and wobbling rotations. These properties are also calculated for the labeled molecule.

Our results show that the pure SA bilayer has a highly ordered periodic structure with a global tilt of the molecules. We found that the introduction of the spin-labeled molecule affects the bilayer in two ways: a localized perturbation that expresses as an increment in the number of gauche defects only in the SA molecules closest to the labeled one and a nonlocalized effect consisting of the increment of the global tilt of the lipids. The spin label order parameters are analyzed and compared with those of the SA molecules.

The mixed SA/cholesterol bilayer showed a structure without long range order and no global tilt of the alkyl chains. This liquid-ordered-like structure shows a higher susceptibility to structural changes when the labeled molecule is incorporated into the system.

Methods

Force Field Parameters Used for Stearic Acid Molecules. The parameters used for SA were GROMOS96 43a2x, extended

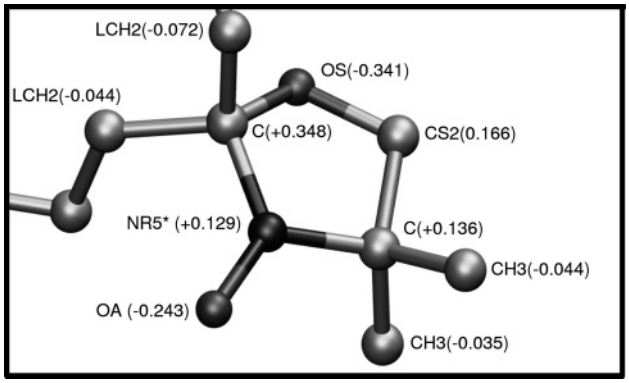

Figure 1. Molecular scheme of the doxyl portion of the labeled SA showing the atom type assignment of the GROMACS force field and the calculated atomic charges used in the simulation.

to better reproduce the behavior of long tail lipids.[26] Explicit hydrogen atoms were used for all polar groups. United atoms were used for the hydrocarbons. For the CH_2 and CH_3 groups of the fatty acids, the Ryckaert−Bellemans torsional potentials were used, which appear to be well suited for membrane simulations, since they can reproduce the experimentally observed trans/gauche ratios for hydrocarbon chains in phospholipids.[27] The SPC model was used for water.[28]

Concerning cholesterol, we adopted the parametrization used in the work of Höltje and Brandt.[19]

Force Field Parameters Used for the 10-Doxil-Stearic Acid Molecule. The doxyl chemical group structure was built using average values of bond distances and bond and dihedral angles obtained from several crystalline compounds reported in the Cambridge Crystallographic Database[29] that contain this group in a similar environment.[30−32] The structure of the labeled lipid was completed attaching the doxyl group to the C10 carbon of a SA molecule. Bonding interactions of the doxyl ring in the SA-labeled lipid were parametrized with the GROMACS force field assigning the atom types shown in Figure 1 (PRODRG server[33]). The rest of the labeled molecule was simulated with the parameters already used for the nonlabeled SA molecule.

The partial charges of the atoms of the doxyl group were obtained from an ab initio Hartree−Fock quantum mechanical calculation with the 6-311G basis set using the GAMESS program[34] and the CHELPG algorithm.[35] To achieve the necessary consistency among the new atomic charges and those already in the force field (default GROMOS96 charges), we also calculated using the same procedure the atomic charges of the carboxylic acid group (for an acetic acid molecule used as a model) and performed a scaling of the novel charges of the doxyl group. The charges thus obtained for the doxyl group are exhibited in Figure 1, and they were used in all MD simulations along with the standard atomic charges of the GROMOS96 force field, for the rest of the atoms. All bonds were constrained by the LINCS algorithm.[36]

Improta et al.[37] have worked out a detailed extension of the AMBER force field to several nitroxide adducts. The results of atomic charges fitted to the electrostatic potentials from quantum mechanical calculations are used to define the parameters in agreement with the philosophy followed by the AMBER force field. They also calculated the hyperfine tensors for those cases. Also, Murzyn et al.[38] have obtained an atomic charge parametrization of a nitroxide adduct for use with the OPLS force field by ab initio quantum mechanical calculations followed by a RESP charges fit.[39,40] An analysis of those calculations shows that the differences among the adducts mainly influence the charge over the N atom. None of those adducts include an oxygen atom in the ring attached to the nitroxide group at variance with our doxyl label. Thus, direct comparison with our results is not straightforward, although the atomic charges obtained in our calculation are within the range spanned by the various adducts in those references.

Initial Configuration of the Pure SA Bilayer (Model A). Because of its well-known stability, we start building a SA molecule using standard angles and bond distances corresponding to all of the dihedrals in the trans conformation. Subsequently, a bilayer of 140 SA molecules (70 in each layer) was prepared with a custom-made program based on the "skew start" method.[41] The SA molecules are inserted in a regular (but not periodic) $x-y$ arrangement, with their long axis pointing perpendicular to the bilayer, that is, parallel to the z axis, with a random rotation around their long axis. The distance between adjacent SA molecules (in the xy plane) was chosen in order to reproduce the 21 Å^2 experimental area per lipid from water−SA−monolayer isotherms of the gel phase[16] (see also refs 17 and 21).

The potential energy of the bilayer array was optimized with a steepest descent method until the maximum force was less than 200 kJ mol^{-1} nm^{-1} in order to preclude for instabilities in the following MD simulation stages due to artificially high forces, as the starting structure was built based only on a geometrical criteria. This same structure was later used also for building the cholesterol/SA bilayer initial stage. All of the MD simulations, annealing procedures, and energy minimizations in the present work were performed using the GROMACS 3.2 package.[42,43]

This bilayer was arranged into a tetragonal cell ($x = 4.069$ nm, $y = 4.166$ nm, $z = 7.50$ nm), keeping the z axes along the normal to the bilayer planes. Water molecules were added until they filled the cell, resulting in 1435 molecules. Finally, the system was minimized using the steepest descent method until the maximum force was less than 200 kJ mol^{-1} nm^{-1}.

We initially performed a simulated annealing of the entire system (fatty acid + water) at high temperature, using MD. This step was done so that the molecules could lose any correlation with the regular initial configuration. This annealing procedure will be described below, and it was applied to all systems as a final step to prepare the initial configuration. After each modification of the bilayer structure and before starting a new MD stage, an energy minimization was performed.

Annealing Procedure. The following annealing protocol was used in order to shorten the equilibration stage of the MD. All models mentioned above were run under the same annealing protocol:

NPT Ensemble (300 K, 1 atm) MD (200 ps). The aim of this stage was to approximate the size of the simulation box to consistent values for the chosen T and P conditions before increasing the temperature. In all MD simulations performed in this work, we used the Berendsen thermostat[44] just to control temperatures within a coupling time of 0.1 ps. A semi-isotropic pressure bath with a coupling time of 4 ps and a compressibility constant of 6×10^{-5} bar^{-1} was used at this stage.[44,45]

NPT Heating from 300 to 350 K (200 ps). The annealing procedure was performed to allow the system to depart from local minima and explore the conformational space of available arrangements in the plane normal to the z direction in a shorter time scale. SA presents an alkyl-chain-melting transition at 343 K, and therefore, the choice of an annealing temperature of 350 K should allow the system to rearrange in the interface plane within a soft constrained environment. Soft restraints in the z direction over the C2 atoms (70 kJ/mol·nm^2) were applied

around the average C2 *z* coordinate to preclude for an excessive and irreversible departure of the lipid from its equilibrium structure during this step. The same parameters of the previous step were used for the *P* and *T* baths. The C5 carbon of the cholesterol molecule and the C1 carbon of the SA* molecule were also restrained when this step was applied to the mixture models.

NPT Cooling from 350 to 300 K (800 ps). The goal of this step was to let the system explore several conformations before arriving at the target temperature of 300 K. This process was made under identical restraints and pressure bath conditions as in the previous step.

The last frame of this step was used as the starting configuration for the subsequent MD runs.

$NP_Z\gamma T$ at T = 300 K, Constant Surface Tension = 1.25 × 10^{-2} N/m (400 ps). The restraints were withdrawn in three consecutive steps (constant force $K = 50, 30, 15$ kJ/mol·nm^2), in order to let the system reach equilibrium at the new pressure. The choice of the most realistic boundary conditions for lipid membrane simulations has been largely under debate in the literature. The constant surface tension ensemble has emerged as a very convenient alternative to determine structural parameters from simulations on frequently used system sizes.[46] Nevertheless, the appropriate value of the surface tension parameter is not an experimentally accessible quantity.[47] Moreover, the appropriate value of the surface tension parameter seems to be dependent on the size of the simulated membrane.[48] In this work, we chose a value of the surface tension to reproduce an experimentally determined area per lipid as obtained in SA monolayer isotherms.[49] It is well-known that the behavior of phospholipid monolayers can be very different from that of bilayers, particularly in the gel phase.[50] However, for some cases, like DMPC in the gel phase, the value of the area per lipid obtained from neutron scattering measurements[51] agrees with that obtained from direct monolayer measurements.[52] In any case, this choice may reproduce approximately the average intermolecular distances found in the experimental system. The last frame of this step was adopted finally as the starting configuration for the subsequent MD runs.

Initial Configuration of the SA/Cholesterol (30%) Bilayer (Model B). The initial configuration and topology of the cholesterol molecule used in this paper were taken from the simulations of mixtures of SA/palmitic acid/cholesterol by Höltje and Brandt.[19]

Starting from the lipid configuration of model A, 20 SA molecules in each monolayer were replaced at random by cholesterol. This lipid configuration (B) was used later to prepare a SA/cholesterol bilayer labeled with 10-doxyl-SA.

Initial Configuration of Bilayers of Pure SA Labeled with 10-Doxyl-SA (Model A*). The last frame of the MD run (300 K) of the pure SA bilayer was used as the starting configuration to introduce one 10-doxyl-SA molecule in each layer. A randomly chosen SA molecule was replaced by one 10-doxyl-SA molecule. After the energy minimization step, the system was annealed under the protocol described previously.

Initial Configuration of Mixed SA/Cholesterol (50:20) Labeled with 10-Doxyl-SA (Model B*). The lipid structure B was used to build a mixed SA/cholesterol (50:20) bilayer labeled with 10-doxyl-SA. Two SA molecules (one from each monolayer) were randomly replaced by 10-doxyl-SA. After the energy minimization step, the system was annealed as stated before.

MD Simulations without Restraints. For each model, production MD simulation runs were performed using the GROMACS package at temperatures of 285, 300, 315, and 330 K, without any restraints. These simulations were run in the $NP_Z\gamma T$ ensemble. The surface tension bath was adjusted with a coupling time of 4 ps and a compressibility constant of 6 × 10^{-5} bar^{-1}.

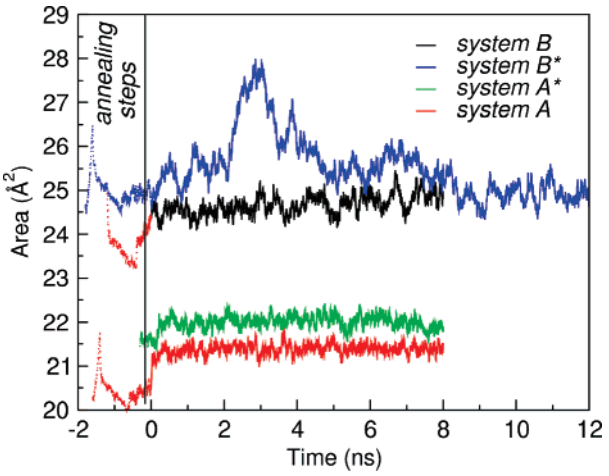

Figure 2. Time evolution of the average area per molecule at 300 K. Negative time values correspond to the annealing stage.

It is well-known that phospholipid membrane simulations starting from arrangements out of equilibrium can require very long times to reach the production stage,[14] particularly if they started from the highly compact and periodic structure of the crystalline phase.[53] For these kinds of systems, equilibration steps from 1.2 ns[53] to 10 ns[14] have been claimed to be necessary. Because of this, we started from a nonperiodic and nontilted structure and let the system relax toward equilibrium after an annealing step of 1 ns and a preliminary equilibration step at the final temperature of 400 ps. Taking into account the fact that the SA molecule is much smaller than PC phospholipids and that we used a long annealing step, we expect the equilibration periods to be much shorter than those quoted above for the present systems. The simulations for systems A, A* and B, and B* were run for 4, 8, and 12 ns, respectively. The properties of interest were calculated over the last 2 ns of the simulations. The simulation of system A was extended by an additional 4 ns period to verify that the averaged properties had converged to trustworthy values. Figure 2 shows the time evolution of the average area per molecule for all systems at 300 K, starting from the annealing stage in the cases it was performed. For nonlabeled systems (A and B), the equilibration times are much longer than those used in ref 19 and assumed to be appropriate. As can be seen from the graph, systems are expected to have reached the equilibrium conditions at the time where the averaged properties are calculated. For system B*, a longer run (12 ns) was unavoidable due to the large fluctuation of the area between 2 and 4 ns. Nevertheless, we verify the convergence for the last 4 ns by following the evolution of the order parameter in intervals of 1 ns (see Figure 1 in the Supporting Information). We also keep track of the time evolution of the fraction of dihedral angles in the trans conformation for SA and verified this property has converged for the last 4 ns of each run (Table 1 in the Supporting Information shows 1 ns partial averages). Systems with labeled molecules deserve particular consideration. The procedure described previously implies that averaged properties of the system, like area per molecule, order parameter, and fraction of dihedral angles in the trans conformation reached well-defined values and fluctuate around them. However, it is important to recall that there is only one labeled molecule in each leaflet of the bilayer. Thus, simulation times required for these molecules

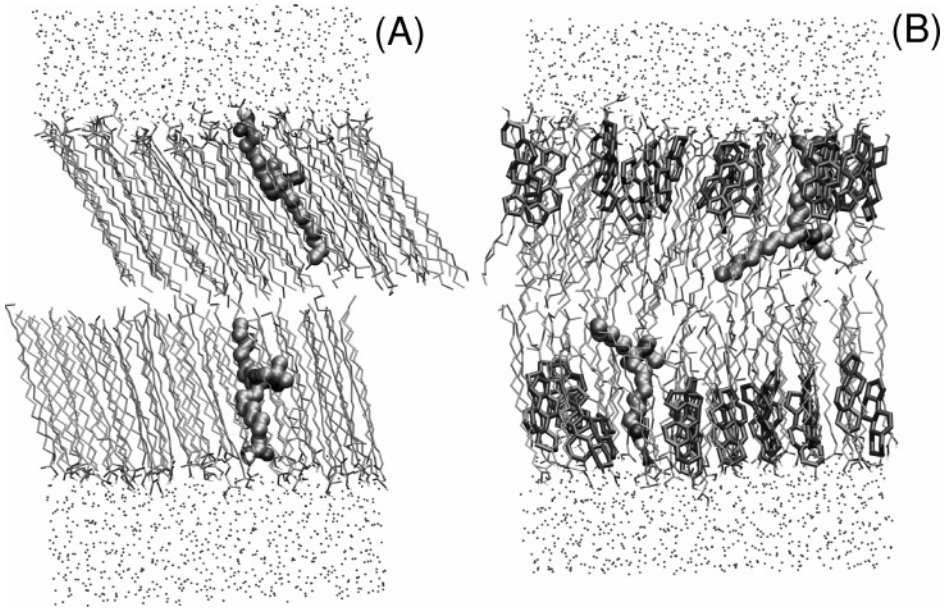

Figure 3. (A) Snapshot taken from the equilibrated MD simulation in the system SA/SA* at 300 K. The point of view of this figure has been chosen to make the angle of tilt of the upper layer appreciable. (B) Snapshot from the MD simulation of the system SA/SA*/cholesterol (300 K). Small points correspond to water oxygen positions, thin gray lines to SA molecules; ball representation to the spin-labeled molecule; and thicker stick representation to the ring portion of the cholesterol molecules.

to laterally diffuse to any of the allowed local environments in the layers were beyond our computational resources, particularly for the SA/cholesterol mixture. Therefore, our approach was to evaluate only locally averaged properties of the labeled molecule due to the short time scale motions within two relevant local environments (one beside a cholesterol molecule and the other in its neighborhood). This means that all calculated properties of the labeled molecule should be understood to have been obtained under this assumption. As the averaged area and global properties of the system are well converged under the conditions of the chosen $NP_Z\gamma T$ ensemble, this is equivalent to follow the motion of the labeled molecule in two relevant and different local environments. These conditions are equivalent to mimic the behavior of different lipid patches around the spin labels that are in equilibrium in real systems. This approach possesses some limitations on the accuracy of the calculated averages over spin label molecule properties. In spite of this limitation, we believe we were able to draw a meaningful picture on the behavior of the spin label in these systems, that has not been previously reported.

Models B and B* did not reach equilibrium at 330 K within the simulation times, and we cannot reject the possibility that under these conditions the bilayer structure became unstable.

Results

Pure and Labeled Stearic Acid Bilayers (A and A* Models). *(i) Analysis of the Average Structure Factor.* Figure 3A shows a snapshot of the equilibrated pure SA bilayer with the spin-labeled molecule at 300 K. A visual inspection of the simulated system reveals a highly ordered structure. We calculated the mean structure factor along the simulation time as a function of the wavenumbers (q_Z, q_{XY}) by averaging over all directions in the *xy* plane (Supporting information).[17,21] This calculation that mimics the results of small-angle X-ray diffraction showed that the SA molecules arrange in a 2-D hexagonal lattice with primitive vectors $a = 4.74$ Å and $b = 5.15$ Å. Our results also show that the SA long axis presents a global tilt of approximately 25°. The tilt was oriented along different azimuthal directions on each leaflet (toward the

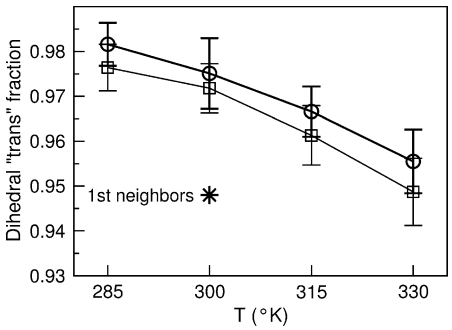

Figure 4. Average fraction of alkyl dihedral angles in the trans conformation for all SA in system A (circles) and system A* (squares). The isolated ∗ symbol in the graph is the fraction of alkyl dihedral angles in the trans conformation averaged only over the SA lipids that are in the first neighbor shell of the labeled molecule at 300 K.

"nearest neighbor" or "next nearest neighbor" lipids in the periodic lattice). Taking into account these properties and the analysis that follows from the conformational order of the alkyl chains, we can characterize this phase as a "condensed phase" in the vocabulary of ref 21, or in the "gel-like phase" as is usual in phospholipid literature.[54]

(ii) Analysis of the Average Fraction of Alkyl Dihedral Angles in the trans Conformation. Now, we turn to the study of the conformational order of the alkyl chains in pure (A) and labeled (A*) SA bilayer systems. Figure 4 shows the averaged fraction of alkyl carbon dihedral angles in the trans conformation for both systems. This averaged fraction was only 0.5% lower in the labeled system than in the pure system at all temperatures.

The question that arises is whether this small change in going from system A to system A* is originated only from a local effect over the molecules around the spin label, or a collective effect. We calculated the average fraction of dihedral angles in the trans conformation for the first and second neighbor shells of molecules around the spin label and for a group of molecules far from it in system A*. At 300 K, the values are 94.8, 97.4, and 97.6%, respectively, which should be compared against the values for the global average value 97.4% for the labeled system and 97.6% for the nonlabeled system. The obtained values show

TABLE 1: Average Inclination Angle (θ), Standard Deviation of Inclination Angle (σ_θ), and Standard Deviation of Azimuthal Angle (σ_φ) of SA's in Systems A (Unlabeled) and A* (Labeled)

	system A (unlabeled)				system A* (labeled)			
	285 K	300 K	315 K	330 K	285 K	300 K	315 K	330 K
θ	24.7°	24.0°	23.9°	23°	26°	27°	26°	26°
σ_θ	0.8°	0.9°	0.9°	1°	1°	1°	1°	2°
σ_φ	2°	2°	2°	2°	1°	1°	2°	3°

that the label produces a small and highly localized increment in the number of gauche defects in its surrounding that essentially affects the first neighbor shell of molecules. The change observed in the global average between the nonlabeled (A) and labeled (A*) systems is a consequence of this inhomogeneity.

(iii) Analysis of the Average Inclination and Azimuthal Angles of the SA Long Axis. The SA molecules in the A and A* systems present a collective tilt of the fatty acid long axes as follows from the snapshot in Figure 3A and also from the structure factor calculation (Supporting information). To study this feature, we follow the behavior of the C1−C18 vector of the SA molecules averaged over the whole system and the time of the simulation. We characterize the tilt with the average inclination angle (θ) sustained between this vector and the normal to the bilayer. The standard deviation of the azimuthal angle of the C1−C18 vectors referred to its mean value in the corresponding leaflet (φ, the angle between the *xy* projection of this vector and the *x* axis) ought to be monitored also to assess that this is really a collective effect.

Table 1 shows the average inclination angle values for systems A and A* at several *T* values. The standard deviation of the inclination and of the azimuthal angle are also quoted. The small value of the azimuthal angle dispersion guarantees that this is indeed a global and homogeneous effect of tilting. The value of the average inclination angle is in agreement with that obtained from the structure factor calculation at 300 K (Supporting information). There is a significant increment of the tilt angle when the spin label is introduced in the system. Both systems present small values of the tilt angle dispersion, that do not change substantially with temperature as follows from these results.

We calculated local averages of the tilt and azimuthal angle for the first and second molecular neighbor shell and for a group of molecules, far from the labeled one, to test whether this is a local effect. We observed that these quantities deviate from the average tilt much less than the difference between the labeled (A*) and nonlabeled systems (A). We then concluded that this tilt change is a collective effect and not a consequence of a local disturbance over the averages.

The present simulations started from the nonperiodic and nontilted structures described in the previous section. The initial configuration of the labeled structure was independent from the unlabeled one. These facts support the statement that the present is not an artifact related to the preparation of the system at the preproduction stage. In what follows, we analyze the origin of the change in the collective tilting of the fatty acids.

(iv) Analysis of the Average Molecular Area. The spin label has a considerably larger molecular volume due to the presence of the doxyl ring. It is then expected that this molecule would not fit in the highly ordered structure of the pure SA bilayer, and give rise to a drop of the cohesion energy in the labeled system. As the current simulations were carried out at constant surface tension, it is then expected that the inclusion of labeled molecules would produce an increase in the average area per SA molecule.

To confirm this hypothesis, we calculated the average area associated with each SA molecule in both systems (A and A*). As we faced the problem of calculating this area for an inhomogeneous system with several molecular species, we used the method proposed in ref 14. The mean area is calculated from the statistical averaged occupancy of the nodes of a grid by a given molecular species in a slice parallel to the interface, along the simulation time. It is important to anticipate that with this method of calculation the total layer area is not the sum of molecular areas, since there are void spaces. The mean area per molecule so calculated is not directly comparable with the values obtained from the simulation box dimensions. Nevertheless, the areas so obtained are a measure of the portion of surface occupied by each molecule, that allow one to make comparisons across systems.

Using these calculations, we found the values of Table 2. The small but significant increase in the area per SA molecule in going from the unlabeled to the labeled system is shown. It is also shown that the area associated with the labeled molecule is sensibly higher than that of the unlabeled SA. These values are consistent with the hypothesis sketched in the above paragraphs. With a larger available area per SA molecule in system A*, an increase in the tilt angle is then expected, which brings the alkyl tails closer to each other to favor their interactions. This effect is appreciable at the spin label composition of these simulations (1.4% concentration of labeled molecules) and would be more pronounced at higher concentrations.

(v) Analysis of the Average Order Parameter Tensor Profiles. We use the "order parameter tensor" (**S**) to characterize the directional order of the alkyl tails at different positions on the hydrocarbon chain.[2] If we take *z* as the direction normal to the bilayer, the diagonal element of the tensor along this orientation is

$$S_{ZZ}(i) = \left\langle \frac{1}{2}\left[3\cos^2(\theta_i) - 1\right] \right\rangle \qquad (1)$$

where θ_i is the angle sustained between the vector that joins C atoms at positions $i - 1$ and $i + 1$ of the chain and the *z* direction. The angular brackets mean time averaging of the enclosed quantity and eventually over all molecules of the species. The quantity to be averaged has a value of $+1$ if the molecular axis points along the *z* direction, and $-1/2$ if it points perpendicular to it. This quantity averages to zero for an isotropic distribution of the local molecular axis, and this fact justifies its use to characterize directional order. Nevertheless, the average orientation of the molecular axis also affects the value of $S_{ZZ}(i)$ that should be taken into account when trying to understand systems where there is a collective tilting of the molecules.

Figure 5 displays the $S_{ZZ}(i)$ profiles along the alkyl chain for the pure (A) and labeled (A*) systems at several temperatures. The graph shows that for both systems and at all temperatures the S_{ZZ} order parameter profile has a characteristic plateau that extends from C4 to C15. The constant values of the order parameter in the plateau region is consistent with the compact and ordered nature of the layer phase. The values of the S_{ZZ} profile at the plateau for system A are not strongly affected by the temperature. The S_{ZZ} decrease toward the headgroup and tail portions of the fatty acid where there are fewer steric constrains and a higher mobility is allowed. There, the values of S_{ZZ} are more sensible to the thermal effects in system A.

TABLE 2: Average Molecular Area of Different Species in Systems A, A*, B, and B* in Å^2 [a]

	SA		cholesterol		
	zone R	zone T	zone R	zone T	SA*
pure stearic acid (system A)	13.33 ± 0.02				
labeled pure stearic acid (system A*)	13.64 ± 0.02				28.28 ± 0.08
mixed stearic acid/cholesterol (system B)	12.75 ± 0.02	14.36 ± 0.03	24.58 ± 0.04	16.37 ± 0.05	
labeled mixed stearic acid/cholesterol (system B*)	13.79 ± 0.03	15.23 ± 0.04	25.00 ± 0.05		38 ± 2

[a] The values are taken from the depth profiles at the positions where they have local plateaus. For systems A and A*, only one zone is present and quoted. In the cases of systems B and B*, values taken from different zones (zone R at the cholesterol ring depths and zone T deeper regions) are quoted. In the case of system B*, the cholesterol profile decreases smoothly and the value in zone T is not well defined.

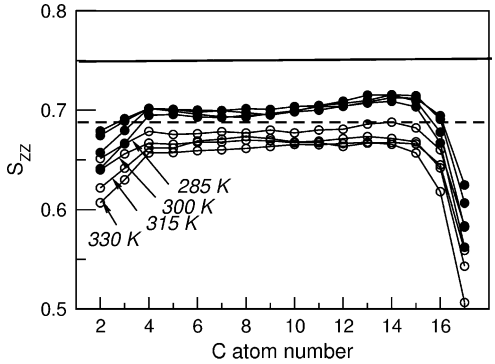

Figure 5. Calculated $S_{ZZ}(i)$ of the SA chains as a function of carbon atom position in systems A (solid circles) and A* (open circles). For the meaning of solid and dashed lines, please see the text.

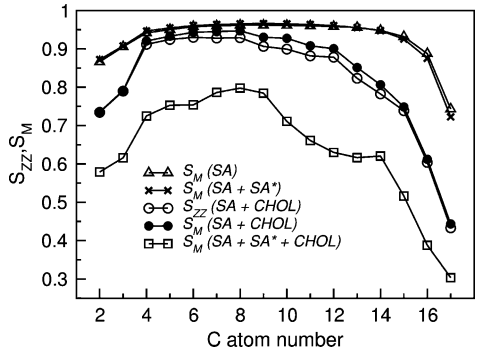

Figure 6. S_{ZZ} and S_M profiles calculated for the SA's in systems A, A*, B, and B* as a function of the carbon atom position in the alkyl chain, obtained from the MD run at 300 K.

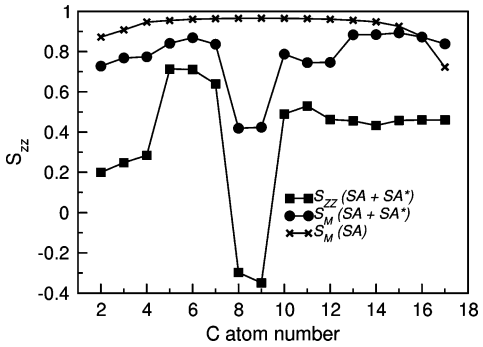

Figure 7. S_{ZZ} (filled squares) and S_M (filled circles) profiles of SA* chains calculated for system A* (SA/SA*) at 300 K. The S_M profile calculated for the SA chain in system A was added for comparison (crosses).

There is a significant change in the S_{ZZ} profiles from system A to A*. The profiles for system A* have lower values than those of system A in the plateau region and also are more sensitive to rising temperatures. These facts are in agreement with a higher average tilt angle in system A*. One obvious question arising is whether this change is related only to the variation of the tilt angle between these systems or to an increased conformational disorder. Two horizontal lines representing the ideal profile expected for an all-rigid-trans carbon chain having their long axis tilted by a constant value (taken as the average angle found for systems A (full line) and A* (dashed line) at 300 K) are also shown for reference in Figure 5. It can be seen that the observed differences between the actual profiles for systems A and A* are smaller than those between the profiles corresponding to the rigid molecules, suggesting they can be entirely explained by the change in the tilt angle.

This hypothesis can be confirmed by diagonalizing the average second rank tensor $\mathbf{S}(i)$ by a convenient rotation of the reference frame. Using this procedure, the principal direction associated with the largest eigenvalue of $\mathbf{S}(i)$, $S_M(i)$, can be found. This principal axis represents the preferred orientation of the C($i + 1$)−C($i - 1$) vectors, and S_M, the largest value of the order parameter associated with this direction. Values of S_M close to 1 mean a highly ordered system along the principal axis. Conversely, values of S_M close to 0 indicate the lack of a preferred orientation. This procedure leaves away the incidence of the tilt angle over the order parameter. Very useful conclusions can be drawn from the joined analysis of the $S_{Z,Z}(i)$ and $S_M(i)$ profiles. Thus, while the former is determined by the average orientation of the molecular axis around the normal to the bilayer and also by other moments in the distribution of these directions (particularly its width), the $S_M(i)$ profiles are only dependent upon the directional dispersion. These allow one to characterize the orientation and motion of the molecules in the system.

Figure 6 shows the largest eigenvalue profiles of the average **S** tensor (S_M) for SA in systems A and A* at 300 K. As expected, these profiles are shifted to larger values than $S_{Z,Z}(i)$ as a consequence of the new reference frame. The most significant feature is that the profiles for the pure (system A, triangle symbol) and the labeled (system A*, cross symbol) systems are now almost coincident. This strongly supports the interpretation that changes in the average tilt angle are the source of the differences between the $S_{Z,Z}$ profiles for systems A and A*. This is also consistent with the values obtained for the average fraction of dihedral angles in the trans conformation, being similar for both systems. On the other hand, the values reached by the $S_M(i)$ profiles reveal the highly ordered nature of the phase in systems A and A*.

We can also analyze the average **S** tensor behavior for the alkyl chain of the labeled molecule in system A* to characterize its orientational order. This analysis is particularly relevant, since the S_{ZZ} behavior at the position of the doxyl ring is directly related to the EPR spectrum of the sample. Figure 7 shows different S profiles as detailed in the captions for the simulation at 300 K. The first feature to point out is that the S_{ZZ} (Figure 7, filled squares) and S_M profiles (Figure 7, filled circles) for the labeled molecule are different from those found for the unlabeled SA molecules ($S_M(i)$ for unlabeled molecules from Figure 6 have been reproduced in Figure 7, crosses). Thus, the former S_{ZZ}

TABLE 3: $S_{Z,Z}(10)$ and $S_M(10)$ Values of Unlabeled SA and Labeled SA* Molecules in System A* at the Simulated Temperatures (The Axial Correlation Times for the Unlabeled SA Molecules in Systems A, A*, and B* Are Also Included)

		temperature		
		285 K	300 K	315 K
pure stearic acid system	$S_{Z,Z}(10)$ of SA	0.67	0.66	0.66
	$S_M(10)$ of SA	0.96	0.96	0.96
	τ^A of SA in system A	22 ps	16 ps	14 ps
	τ^A of SA in system A*	22 ps	15 ps	12 ps
	$S_{Z,Z}(10)$ of SA*	0.62	0.35	0.19
	$S_M(10)$ of SA*	0.87	0.83	0.61
mixed stearic acid/cholesterol system	$S_{Z,Z}(10)$ of SA	0.83	0.75	
	$S_M(10)$ of SA	0.85	0.75	
	τ^A of SA in system B*	51 ps	47 ps	
	$S_{Z,Z}(10)$ of SA*	0.07	0.74	
	$S_M(10)$ of SA*	0.78	0.77	

profiles did not follow the features of those corresponding to the nonlabeled SA molecules. The same general behavior was also observed for the rest of the simulation temperatures. We have also compared these S_{ZZ} profiles with those of SA belonging to the first neighbor shell of the labeled SA molecule and found they are also remarkably different (not shown).

We observe that the general shape of the $S_{Z,Z}$ (Figure 7, filled squares) and S_M profiles (Figure 7, filled circles) for SA* presents similar trends, being the last shifted to higher values due to the local change in the reference frame. The analysis of the $S_{Z,Z}$ profiles of the labeled molecule within different time intervals reveals that important conformational changes occur in times in the order of 1 ns.

Keeping in mind the above discussion, we can conclude that C8 and C9 of the alkyl chain of the labeled molecule have the largest dispersion in orientations out its molecular axis (lowest values of $S_M(i)$ order parameter). Beyond the C10 position, there are also values of $S_M(i)$ that indicate a significant dispersion of axis orientations at C10−C12 but much lower that those at C8−C9. The $S_{Z,Z}$ profile does not show the same behavior at C10−C12, since changes in the average orientation of these atoms compensate for the dispersion effects. It is also seen that C10, which is attached to the doxyl ring, has a lower mobility than C11−C12 which are deeper toward the tail of the chain.

The $S_{Z,Z}(10)$ order parameter, corresponding to the position where the doxyl ring is attached, decreases when the temperature rises (see values in Table 3).

The observed time fluctuations in the $S_{Z,Z}$ graphs of the probe lead us to inquire whether one could relate an S profile calculated from a small time interval to a particular set of conformations of the labeled molecule. If this were the case, the $S_{Z,Z}(i)$ profile could be obtained as a weighted superposition of component profiles each associated with different molecular conformations of the spin-labeled molecule. We performed a statistical cluster analysis using the Daura et al. algorithm,[55] to identify several sets of conformations of the labeled molecule. To clusterize the molecular conformations, we used a root mean square deviation (rmsd) criterion with a suitable cutoff. Our objective was to identify the different conformational sets, and also to study the population of these sets when the temperature changes. Thus, the statistical cluster analysis was done over the whole group of trajectories simulated at different temperatures. Figure 8 shows a sketch of the most representative molecular geometries found in our statistical analysis.

From the statistical cluster analysis, it follows that the lowering of the $S_{Z,Z}(i)$ profile at 300 K between C2 and C4 (see Figure 7) can be associated with an increasing participation of cluster 2. If one looks at the molecular sketches in Figure 8, it is then clear these features on the profiles are mainly associated with the changes in the orientation of the local molecular axis in the neighborhood of the polar head. Conversely, the S_M profile (see filled circles) does not show such a large drop. The molecular conformation of this cluster exhibits an enhanced electrostatic interaction between the doxyl ring and the polar head due to their proximity. At lower temperatures, this component has a smaller participation because of the difficulties in arranging this molecular geometry in such a compact structure. At higher temperatures, the entropic contribution dominates over the energetically favorable interaction, and the participation of this component also decreases.

Conversely, the drop of $S_{Z,Z}(i)$ and $S_M(i)$ at C8−C9 is common to both profiles. This suggests they are derived from an orientational dispersion rather than an average reorientation of the local molecular axis. The presence of the doxyl group in the labeled SA* produces an important disruption in the energetically favorable regular packing of the membrane, as was discussed in the analysis of the area data. The labeled molecule introduces localized and dynamic gauche defects into positions C8−C9 and to a lesser extent at C10−C12 to arrange such perturbation in an energetically less unfavorable way. A local increment of the trans−gauche transitions at these positions also shows that this is the case. The analysis of the $S_{Z,Z}$ and S_M profiles of the SA molecules surrounding the labeled one shows that only the first neighbor shell is perturbed (as discussed above). Nevertheless, the cohesion energy is also affected by the perturbation, as discussed in the section devoted to the area result, leading to the nonlocal effect over the area and global tilt of the bilayer at the label concentration where the simulation has been performed. At 315 and 330 K, the contribution of cluster 3 becomes more relevant because of the activation of additional gauche defects close to the doxyl ring.

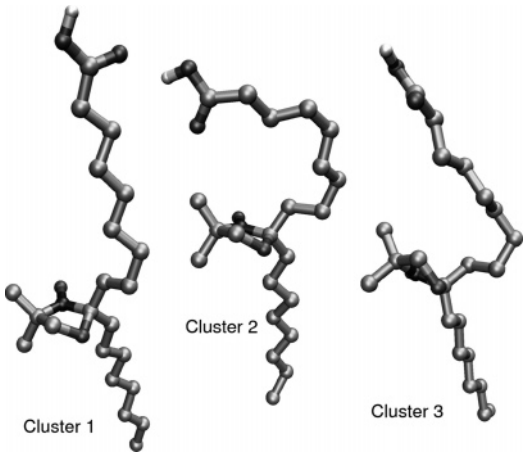

Figure 8. Representative molecular structures of the spin-labeled SA molecule for the principal clusters found in the MD trajectory of system A*.

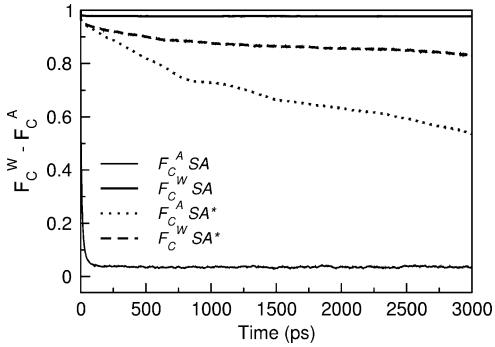

Figure 9. Wobbling (F_C^W) and axial (F_C^A) autocorrelation functions for SA and SA* in system A* at 300 K.

Table 3 summarizes the values of $S_{Z,Z}(10)$ and $S_M(10)$ of the unlabeled (SA) and labeled (SA*) molecules, at several temperatures. It can be seen that the $S_{Z,Z}(10)$ and $S_M(10)$ values for unlabeled SA molecules in the gel-like system (A or A*) do not depend on temperature in the simulated interval. As it was already pointed out, $S_M(10)$ values are larger than $S_{Z,Z}(10)$ values due to the tilting effect. However, the $S_{Z,Z}(10)$ and $S_M(10)$ values for the labeled SA* molecule show a significant decrease as the temperature rises. The stronger dependence on temperature exhibited by $S_{Z,Z}(10)$ in the SA* molecule by contrast with $S_M(10)$ means that the distribution of orientations of the C($i+1$)−C($i-1$) molecular axis of the SA* is changing its average as well as its fluctuations. That axis would orient with larger average inclination angles at higher temperatures. The dispersion of this angle also increases with temperature, as can be followed from the change in the $S_M(10)$ values. From these results, one can conclude that both $S_{Z,Z}(10)$ and $S_M(10)$ of the labeled molecule (SA*) are very sensitive to temperature changes, although they do not follow the order parameter variations of the unlabeled SA molecules, at least in this gel-like phase.

(vi) Analysis of the Average Angular Autocorrelation Functions and Correlation Times. The motion of the alkyl chains of SA and labeled SA* molecules can be characterized following the angular autocorrelation function of appropriate vectors. For unlabeled SA molecules, we define a vector $\mathbf{n}(t)$ pointing from C($i-1$) to C($i+1$) and a vector $\mathbf{p}(t)$ pointing normal to the plane defined by the positions C($i-1$), C(i), and C($i+1$). Strictly speaking, the $\mathbf{p}(t)$ vector characterize the rotation around the C($i-1$)−C($i+1$) axis. However, taking into account the high fraction of dihedral angles in the trans conformation as well as the high values of the $S_M(i)$ profiles, one can use $\mathbf{p}(t)$ to survey the axial rotation around the principal axis of the molecule. We will refer to them as "wobbling" (F_C^W) and "axial correlation functions" (F_C^A). In systems A and A*, the unlabeled SA autocorrelation functions were evaluated performing the temporal average over all unlabeled molecules.

For the labeled SA molecule, we define a vector normal to the doxyl ring ($\mathbf{n}_D(t)$), and the other parallel to this plane ($\mathbf{p}_D(t)$). The autocorrelation function $\langle \mathbf{n}_D(t') \cdot \mathbf{n}_D(t'+t) \rangle$ characterizes the wobbling motion of the normal to the doxyl ring around their average inclination angle. On the other side, the function $\langle \mathbf{p}_D(t') \cdot \mathbf{p}_D(t'+t) \rangle$ characterizes the motion of the label group of the molecule in the plane of the doxyl ring. We note here that the autocorrelation functions of vectors $\mathbf{n}_D(t)$ and $\mathbf{p}_D(t)$ are not necessarily associated with the wobbling and axial motion of the alkyl chains of the label due to the presence of gauche defects. Nevertheless, these motions are those surveyed by EPR.

Figure 9 shows the unlabeled SA and labeled SA* autocorrelation functions. For the unlabeled SA, the autocorrelation functions defined previously at the position of C10 have been analyzed after averaging over all SA molecules. The wobbling SA's (F_C^W) show the typical behavior of a gel phase system, in which the tumbling of the long molecular axis is inhibited by the compact structure of the layer. The axial correlation function presents features that are different from those found for phospholipids in the gel phase. This is because the SA molecules are able to rotate as a whole due to the small volume of its head.[56] F_C^A of the alkyl chains has very short correlation times, as quoted in Table 3. It can be observed that the axial correlation times of unlabeled SA decrease as the temperature rises. This trend is observed in both system A and A* bilayers. The correlation times in the labeled bilayer are slightly lower as a result of the larger area available to each lipid, as has been already mentioned.

We have verified that $S_{Z,Z}(10)$ of the labeled molecule SA* gives the same value as that obtained from the evaluation of eq 1 for the angle sustained between the vector $\mathbf{n}_D(t)$ normal to the doxyl ring and the bilayer normal. We assumed that the orientation of the spin unpaired p-like orbital of the labeled group, and therefore the eigenvector corresponding to the largest eigenvalue of the hyperfine coupling tensor, points normal to the doxyl ring.[2,37] Under this assumption and assuming also an axially symmetric coupling tensor, the position of the hyperfine components of the EPR spectra can be written in terms of the angle sustained between the magnetic field and the vector $\mathbf{n}_D(t)$ similarly to eq 1.[57] Therefore, for bilayer samples oriented normal to the magnetic field direction, the positions of the spectral lines are related to $S_{Z,Z}(10)$ of the labeled molecule. Nevertheless, for the spectra calculations, the relation between the characteristic time of the spectroscopy technique and that of the motion of the label comes into play and must be taken into account. This last subject is out of the scope of the present work. For sample bilayers oriented with other angles relative to the magnetic field, a rotation of the **S** tensor must be considered. In the case of nonoriented samples (e.g., vesicles), usually the spectra can be taken as a superposition of those that correspond to different bilayer orientations. Although the values of $S_{Z,Z}(10)$ of the labeled molecule SA* do not follow those of unlabeled SA, they are very sensitive to the changes in their axial correlation times. It is then concluded that the $S_{Z,Z}(10)$ values of SA* and therefore the EPR spectra that are related to them would sense the axial correlation times of the unlabeled lipid molecules in this gel-like phase.

From the first portion of F_C^W for the labeled SA* and assuming an exponential decay, a correlation time of $\tau_D^W \sim 37$ ns can be estimated at 300 K. For this case, the SA* wobbling motion of the doxyl ring is only partially restricted by the global order of the layer. The SA* axial correlation times of the doxyl ring are sensitively larger than those of the unlabeled SA ($\tau_D^A \sim 8$ ns at 300 K). Both correlation times decrease as the temperature rises. The presence of the doxyl group makes the rotation of the labeled molecule around the long axis more difficult, due to its volume and also because the curvature adopted by its alkyl chain. Therefore, the τ_D^A values are notably larger than those for the unlabeled SA molecules. Conversely, the dynamic effects introduced by the gauche defects on the alkyl chain as to arrange the doxyl ring within the compact structure of the bilayer will produce an enhanced motion of the doxyl ring normal. Therefore, the F_C^A value of the doxyl ring decays faster than that for unlabeled SA molecules. The values of τ_D^A and τ_D^W represent only a rough estimation, since the simulation times were not long enough as to allow for their determination.

TABLE 4: Average Fraction of Dihedral Angles in the trans Conformation in Unlabeled SA Chains

T	system A (SA)	system B (SA/cholesterol)	system A* (SA/SA*)	system B* (SA/SA*/cholesterol)
285 K	98.3%	90.5%	97.4%	90.0%
300 K	97.6%	89.0%	96.9%	86.0%

Unlabeled (B) and Labeled (B*) Stearic Acid/Cholesterol Bilayers. The SA−cholesterol mixture (50:20), with and without including the labeled molecule, was simulated at 285 and 300 K, at a surface tension of 1.25×10^{-2} N/m. Due to the lack of experimental data allowing for a meaningful choice of the surface tension for this system, we decided to perform the simulations adopting identical conditions at which system A were run. This arbitrary choice differs from that by Höltje et al. of ref 19, that simulate the bilayer with and without cholesterol by adopting identical conditions, working under isotropic pressure which is equivalent to taking a vanishing value for the surface tension. Our choice to perform simulations on systems with and without cholesterol at the same value of the surface tension allows us to analyze the fluidizing effect of this sterol. The fluidizing effect of cholesterol over the gel phase is well-known in phospholipid bilayers.[13] For the stratum corneum and its mixture of fatty acid models, the same effect has been measured by FTIR and NIR-FT Raman spectroscopies.[19] For the surface tension used in our simulations, the systems reach the equilibrium and were stable along the simulation times at both $T = 285$ and 300 K.

The snapshot of Figure 3B had already shown that the molecular order in these systems is of a completely different nature than that for pure stearic acid bilayers. In this case, there is a complete lack of long range periodic molecular order. Therefore, the analysis of the average structure factor brings no relevant information. Consequently, although item i will be skipped below, the section numbering will be kept so as to follow the same ordering structure as that used for systems A and A*. The bilayer becomes slightly thinner than for system A in spite of the fact that the long axis inclination angles of the lipids are lesser than those found for A. As shown below, the average number of gauche defects per molecule increases while the values of $S_{Z,Z}$ decrease. Thus, the system stays in a sort of liquid-ordered phase resembling that postulated for phospholipid−cholesterol mixtures.[23,24]

(ii) Analysis of the Average Fraction of Alkyl Dihedral Angles in the trans Conformation. Table 4 compares the values of the average fraction of dihedral angles in the trans conformation for the SA alkyl chains across various systems at two temperatures. The values obtained for B (SA/cholesterol) are smaller than those found for pure stearic acid systems. To appreciate the changes in magnitude, we recall that an 8% variation on the fraction of dihedral angles in the trans configuration implies on the average one extra gauche defect per molecule, approximately. This does not necessarily mean there is only one defect per alkyl chain, although an isolated gauche dihedral is much more feasible in this case than it was in the very compact A/A* systems. Thus, the incorporation of cholesterol into stearic acid bilayers produces a substantial increase of the dihedral angle disorder of the alkyl chains. The insertion of the labeled molecule induces a further decrease of the average fraction of dihedral angles in the trans conformation. The notable drop in these values for B* at 300 K, neither observed at 285 K nor in pure SA systems, can anticipate the instability of systems B and B* at higher temperatures. Nevertheless, the fractions of dihedral angle in the trans conformation for system B/B* are much higher than those observed in the liquid crystalline (LC) phases of phospholipids.

TABLE 5: Inclination Angle (θ), Standard Deviation of Inclination Angle (σ_θ), and Standard Deviation of Azimuthal Angle (σ_φ) of SA's in Systems B and B*

	without SA* (system B)			with SA* (system B*)		
	285 K	300 K	315 K	285 K	300 K	315 K
θ	8°	8	8°	5°	11°	9°
σ_θ	1°	1°	2°	1°	2°	2°
σ_φ	111°	111°	90°	117°	222°	173°

(iii) Analysis of the Average Inclination and Azimuthal Angles of the SA Long Axis. Table 5 shows the inclination angle sustained between the average C1−C18 vector of the SA molecules and the normal to the layer. The standard deviation of the azimuthal angle of this vector is also shown. The large value of this last quantity means that there is no collective tilting of the SA molecules, as could have been anticipated from the snapshot of Figure 3B. The inclination angle is significantly lower for this mixture system than it was for the pure system where tilting was present (see Table 1). The inclination and azimuthal angle were obtained averaging over all unlabeled SA molecules and over the simulation time. The effects of cholesterol on the inclination angle of phospholipid bilayer have been discussed in ref 58. They found a cholesterol inclination angle of 19.7° for DPPC mixtures at 323 K that should be compared with a tilt of 32° measured in the gel phase of pure DPPC bilayers.[59] For cholesterol at 300 K, we found an average inclination angle of ~8° for their ring moiety that is coincident to their homologous of SA (see Table 5) that should be compared with that of system A in Table 1 (24° at 300 K).

(iv) Analysis of the Average Molecular Area. The mixed cholesterol−SA system (system B) has *z* profiles that depend sensitively of the depth in the layer. There are two regions involved: one that coincides with the ring location of the cholesterol molecule (called zone R in Table 2) and the other below it (zone T). Table 2 summarizes the results for the labeled and unlabeled systems. The values quoted in this table have been taken from averages of the profile values in zones where there are local plateaus. From Tables 2 and 5, it is seen that the lowering of the inclination angle in going from system A to B can be associated with a decrease in the area per SA molecule at the depth below the cholesterol ring portion. It is also worth noting that the width of the bilayer (measured between averaged hydroxyl-oxygen positions on both leaflets) changes from 42.7 ± 0.2 to 40.7 ± 0.3 Å in going from system A (without cholesterol) to system B (with cholesterol).

From the values in Table 2, it is seen that the introduction of a labeled molecule produces a remarkable enhancement in the average area per molecule of SA and cholesterol, under the constant surface tension conditions of the present simulation. The increase in the average area for SA is even larger than that produced in the gel-like systems A/A*. The region of the *z* profile exhibiting the smallest average areas of SA coincides with that where cholesterol molecules have their largest areas due to their ring moiety (zone R). The opposite is found for zone T. It is worth mentioning that the introduction of the labeled molecule produces important changes at the analyzed concentration, despite the fact that this is a very disordered phase (liquid like). The average SA areas in systems A* and B* are very similar, although their phases are of a very different nature.

(v) Analysis of the Average Order Parameter Tensor Profiles. Figure 6 shows the $S_{Z,Z}(i)$ (open circles) and $S_M(i)$ (filled circles) profiles for SA molecules in system B. These profiles are almost coincident, as a consequence of the small long axis inclination

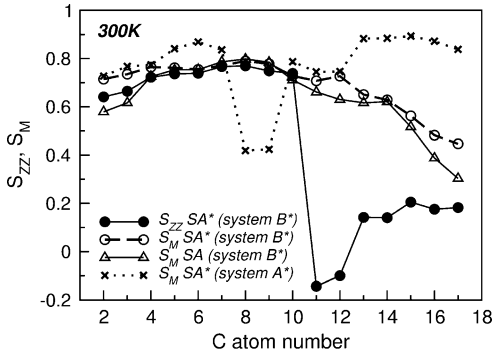

Figure 10. $S_{Z,Z}$ (filled circles) and S_M (open circles) profiles of labeled SA* chains for system B* (SA/SA/cholesterol) at 300 K. The $S_M(i)$ profiles of unlabeled SA molecules in system B* (triangles) are also shown. For comparison, the $S_M(i)$ profiles of labeled SA* in system A* (crosses) have been included.

angle of the SA molecules when cholesterol is present. These values are also lower than the profile of S_M for system A (also shown in Figure 6, crosses), in agreement with the higher conformational disorder of SA molecules in system B. The insertion of the labeled molecule in system B (open squares) causes an appreciable change in the order parameter profiles of the SA molecules, as can be seen in Figure 6. As it was already noted, this is evidence of the important destabilization effects of the labeled molecule in spite of its low concentration.

For the average order parameter tensor of B*, we performed a similar analysis from that performed on system A*. Figure 10 shows the profiles of $S_{Z,Z}(i)$ and $S_M(i)$ for the labeled molecule. These two profiles are very different between C11 and C18 carbon atoms. The differences between $S_{Z,Z}(i)$ and $S_M(i)$ of the labeled molecule signal a change in direction of the long axis at C11. One can suspect from Figure 3 that it is possible for the labeled molecule to position itself below the ring moiety of cholesterol to satisfy its steric constraints in this region of lower atomic density. The S_M profile of the labeled molecule for system A* is also reproduced for comparison. As is evident, the new profiles do not have the lowering found in system A* at the positions C8 and C9. This fact is also in agreement with the previous hypothesis, as the labeled molecule would have no need to introduce costly gauche defects to fit below the region of cholesterol rings.

To understand the above-mentioned differences, we performed the same cluster statistical analysis made for system A*. In the present case, we found two conformational sets (clusters 1 and 2) having the largest populations within the whole group of simulations. Figure 11 shows molecular drawings of a representative geometry of each set. Both structures have a change in the direction of the long axis of the SA* molecule at the position of C10 and have no gauche defects at positions C8−C9, as was the case for the A* system.

The abrupt change of the $S_{Z,Z}$ profile of the labeled SA* from positive to negative values at carbons C10−C11 (Figure 10) shows that beyond this position the molecular axis orients in a direction closer to perpendicular to the bilayer normal. This picture agrees with the molecular conformations found in the cluster analysis (Figure 11).

In the pure stearic acid bilayer (system A*), steric constraints led the labeled molecule to introduce gauche defects to fit into the compact layer structure. In the case of system B*, the cholesterol molecules could take the role of spacers to accommodate the doxyl ring. Figure 12A shows an atomic partial density depth profile of the bilayer that has been divided in slices parallel to the surface. It shows the position distribution

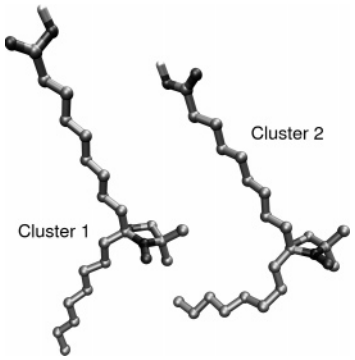

Figure 11. Molecular structure of the two most populated conformational sets of the spin-labeled stearic acid molecule in the system SA/cholesterol.

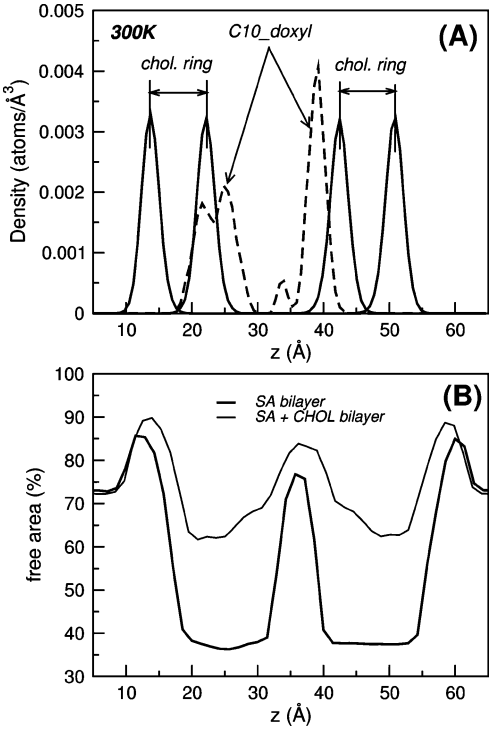

Figure 12. (A) Number of atoms *z* profile for carbon C5 and C21 of cholesterol molecules (full line), which define the average position of the cholesterol ring and for C10 of SA* (dash line) which define the doxyl ring position. (B) Free area calculated for system B (SA/cholesterol) (bold line) and system A (SA) (thin line) both at 300 K.

of (a) the C10 of the labeled molecule where the doxyl ring is attached to the chain and (b) the upper- and lowermost C atoms of the ring portion of the cholesterol molecule. The latter two profiles serve to indicate the zone where the ring moiety of the cholesterol molecules are located along the simulation. The C10 of the labeled molecule profile captures the positions of the doxyl ring. There is a difference in the behavior of this position profile between the two layers. A closer examination over the simulation trajectory led us to establish that this behavior is a consequence of the relative distance between the labeled and cholesterol molecules. When the labeled molecule is next to cholesterol, then the doxyl ring arranges below its ring portion (see Figure 12A, 30 Å $\leq z \leq$ 55 Å). Conversely, when the labeled molecule is near but not beside cholesterol (see Figure 12A, 10 Å $\leq z \leq$ 30 Å), the doxyl ring position fluctuates around the border positions of its ring moiety. This behavior can be seen in the density profile for the C10 of the labeled molecule that in this last case exhibits two peaks.

Figure 12B shows the depth profile for the percentage of area not occupied by molecules (free space) calculated from the grid procedure already mentioned above. It can be observed that, below the position of the cholesterol rings, the fraction of space free from molecular occupancy starts to rise. Thus, it can be concluded that the labeled molecule arranges its doxyl ring and the rest of its alkyl tail, preferentially below the cholesterol rings where more free space is available. There, the labeled molecule may change the direction of the long axis (see Figure 11) without the need to resort to gauche defects. This bend agrees with the abrupt change in $S_{Z,Z}(i)$ of the labeled molecule, that does not appear in its S_M profile (Figure 10, up triangles). Nevertheless, the smooth lowering shown by this last profile is also indicative of a higher mobility of the alkyl tail which is consistent with the above picture.

We have already seen that the fraction of SA dihedral angles in the trans conformation is smaller for system B than for system A, which is evidence of a higher conformational disorder for the former. This disorder is produced by the introduction of cholesterol into the mixture. One relevant question is whether the cholesterol changes the conformational SA order homogeneously along all of the alkyl chains. We have calculated the fraction of SA dihedral angles in the trans conformation at 300 K for system B with several variants: (a) taking into account all of the chain dihedral angles (89 ± 1%), (b) taking into account only the dihedrals from C1 to C9 that statistically stay at depths close to the ring portion of cholesterol molecules (92 ± 0.3%), and (c) taking into account only the dihedrals from C9 to C18 that statistically lay deeper than that of the ring region of cholesterol molecules (87 ± 0.3%).

These significant differences show that the cholesterol molecules produce an increased conformational disorder at depths below their ring portion due to the increment in free space. Conversely, these molecules enhance the conformational order at the depth of their ring moiety. This picture is also consistent with the average molecular areas of each species presented in Table 2. These allow us to assign a spacer or wedge role to these molecules. A hypothesis similar to the present has been used to rationalize the effect of cholesterol in the permeation of O through DPPC membranes by the kink transport model.[60] Our results give support to this picture at least for the SA−cholesterol system.

Table 3 shows that the values of $S_{Z,Z}(10)$ and $S_M(10)$ for the unlabeled SA molecules are much more sensitive to temperature than they were for the pure SA bilayer (systems A and A*). This feature also characterizes the nature of this phase. The analysis of the change of $S_{Z,Z}(10)$ and $S_M(10)$ for the labeled molecule SA* with temperature is not very conclusive due to the magnitude of their fluctuations in the simulated time and the limitations that were discussed in the Method section of this work. However, it is worth mentioning that very different values of $S_{Z,Z}(10)$ are obtained for the labeled lipid at 285 and 300 K (see Table 3). As $S_M(10)$ did not show such temperature changes, this dependence is related to the mean orientation of the doxyl ring, and not to its dispersion. At 285 K, the C10 is positioned well below the ring moiety of cholesterol, as is obtained from a density profile at that temperature (not shown). Under such conditions, the doxyl ring arranges with an average inclination angle of its normal of ∼55°. At 300 K, the labeled molecule is shifted toward the bilayer outer surface, as can be seen by comparing the lower and higher temperature density profiles of C10 and also for the C1 head position. This shift pulls the doxyl group to the zone of the ring moiety of cholesterol where less free space is available, and then, it must arrange with higher steric constraints. In this situation, the average inclination angle of the doxyl normal is ∼21°. These facts explain the increase of $S_{Z,Z}(10)$ of the labeled molecule as the temperature rises. In spite of the fact that longer simulations are needed to sample with accuracy these different situations, the present work shows that this effect is present and should be taken into account when interpreting EPR results.

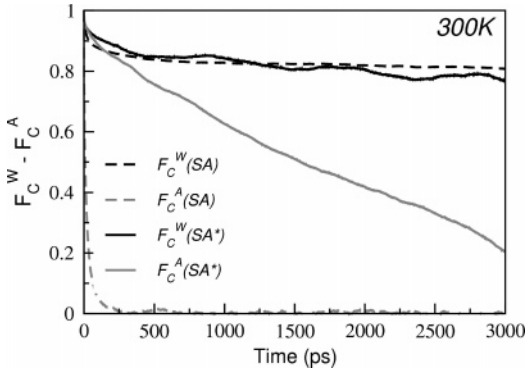

Figure 13. Wobbling and axial autocorrelation functions for SA and SA* in system B* at 300 K.

(vi) Analysis of the Average Angular Autocorrelation Functions and the Correlation Times. Finally, we repeated the analysis of the autocorrelation functions of the SA molecules that we performed previously for the pure SA system. At this point, we note that the behavior of a particular SA molecule will be different if it is near cholesterol molecules or not in contact with them. Nevertheless, we have chosen to analyze its average value over all unlabeled SA molecules. Figure 13 shows the axial and wobbling autocorrelation functions for the SA molecules. The larger number of gauche defects affect the straightness of the SA molecules, and in consequence, they rotate more constrained.

The wobbling autocorrelation function of the labeled SA* for this phase is very similar to that of the unlabeled molecules at short times (see Figure 13). The estimated wobbling and axial correlation times for the labeled SA* molecules are respectively $\tau_D^W \sim 24$ ns and $\tau_D^A \sim 2$ ns, which are both smaller than the corresponding values in the gel-like phase.

Summary and Conclusions

For the pure SA bilayer, we found that the system is in a gel-like phase, with a long range hexagonal periodic order and a collective tilt of the alkyl-chain long axis with azimuthal orientation toward the NN (nearest neighbor) or NNN (next nearest neighbor) directions. In this phase, we found that the insertion of the labeled molecule produces only a very localized perturbation of the fraction of alkyl dihedral angles in the trans conformation, limited to a first neighbor shell. Conversely, there is a significant increase of the molecular area per lipid over the whole layer at the simulated constant surface tension conditions used here. Associated with this growth of the area, there is an increase of the long axis tilt angle of the alkyl chains that brings them closer to each other. The compact structure of this phase produces a plateau of high values in the $S_{Z,Z}(i)$ order parameter profiles of SA molecules between C4 and C15, which decrease toward the head and the tail of the fatty acid molecules.

It is remarkable that such a small addition of spin labels (1.4%) can modify the global properties of the system under constant surface tension conditions. Preliminary results of simulations under similar conditions of those presented here, but with concentrations lower than 0.4%, did not show such a significant change in the tilt angle after the addition of the

labeled molecule. However, what is important to mention is that the perturbing effect of the labeled molecule can be important below the concentration where dipolar or exchange magnetic interactions are negligible for experimental observation.[3,22]

We found that the spin-labeled molecule makes trans−gauche transitions mainly at the C8−C9 positions to arrange the end of the alkyl tail into the compact periodic structure of SA molecules. This kind of behavior has been conjectured in connection with "crankshaft modes" to explain the motion of doxyl labels in compact structures.[4,3] We have found out how these defects appear to arrange the labeled molecule in the compact gel-like structure through our statistical cluster analysis.

The values of the $S_{Z,Z}(10)$ and $S_M(10)$ order parameters of the labeled molecule at the position where the doxyl ring attaches are very sensitive to the temperature changes at variance with those of the unlabeled SA that are almost constant. It is relevant to remark that the $S_{Z,Z}(10)$ parameter of the labeled molecule does not follow the behavior of the order parameter of the unlabeled molecules, as could be assumed.

The axial correlation times of the unlabeled SA molecules decrease with the temperature rise in this rotamer phase. A relevant conclusion of our work is that the values of $S_{Z,Z}(10)$ of the labeled SA*, and eventually the EPR spectra, would measure this lowering of the axial correlation times of the unlabeled lipid molecules in this gel-like phase. The labeled molecule changes its $S_{Z,Z}(10)$ and $S_M(10)$ values due to the reorientation and motion of the doxyl ring. The alkyl chain of the labeled molecule introduces gauche defects to allow such reorientation in the compact structure of the environment, as can be seen from the statistical cluster analysis. Nevertheless, the probability of these defects is dependent on the characteristic motion of the host system molecules that surrounds the label. These facts explain the mechanism by which the labeled molecule surveys the dynamics of the host system for this compact phase. This conclusion gives support to the analysis made in refs 3 and 4 to explain the experimental observations. It is possible that molecules labeled at positions closer to the head (5-doxyl) or tail (16-doxyl) of the alkyl chain would arrange their doxyl rings at the average depth of the head or tail of the host system in order to reduce the steric constraints. Our own preliminary results showed these effects. In these cases, the mechanism by which the labeled molecule surveys the dynamics of the layer should be different.

For the SA−cholesterol mixture bilayer, we found a phase with no long range periodic order. There is no collective tilt of the long molecular axis of SA molecules. The fraction of alkyl carbon dihedral angles in the trans conformation is notably lower than that for the pure bilayer (system A) but higher than those found in liquid crystalline phases of phospholipids. We can then describe the phase as liquid-ordered-like in the nomenclature used in phospholipids. The presence of cholesterol leads to a lowering of the long axis inclination angle of SA and an associated decrease of the average molecular area of SA at the depth of the cholesterol ring moiety. The insertion of the labeled molecule produces a larger increment of the average areas than in system A, in spite of the fact that it is a much more disordered phase. Since the order parameters of SA molecules are not affected by a tilting of the molecular long axis, their $S_{Z,Z}$ and S_M profiles are almost congruent. The insertion of the labeled molecule produces a significant lowering of the S_M profile also for this disordered system.

The analysis of the $S_{Z,Z}(10)$ and $S_M(10)$ profiles of the unlabeled SA molecules shows that these quantities are much more sensitive to the change of temperature in this phase than they were in the pure SA gel-like bilayer (system A). The presence of cholesterol produces a conformational ordering effect (a higher fraction of dihedral in the trans conformation) on the SA at the depth of its ring portion. Conversely, cholesterol enhances the number of gauche defects in SA at depths below its ring portion due to the larger free space it leaves available.

The labeled molecule arranges its doxyl moiety below the ring portion of cholesterol. This fact allows the label to accommodate its tail in a region with larger amounts of molecular free space, without the need to resort to gauche defects. The $S_{Z,Z}(10)$ values for the labeled molecule increase with the temperature rise. This fact leads to an increment of the orientational contribution to the width of each hyperfine component of the EPR spectra. The increment of $S_{Z,Z}(10)$ is originated in the change of average orientation of the doxyl ring. This average reorientation is produced by the change in the depth of the labeled group when temperature rises, that lead it to a zone with the higher steric constraints of the cholesterol ring moiety. It is relevant to note that this kind of effect in the analysis of the temperature dependence of EPR spectra is often missed, and could be particularly relevant with those molecules which are labeled at the central positions of the alkyl chain. Longer simulations are needed to understand the mechanism by which the label surveys the dynamics in these kinds of systems. In spite of the fact that the model systems studied in this work have many properties that make them different from the phospholipid bilayer, we believe that the conclusions we arrived at are relevant to the analysis of EPR experiments on model biomembranes.

Acknowledgment. We are grateful to Prof. A. M. Gennaro and M. C. G. Passeggi for a careful reading of the manuscript and useful suggestions. A.S.G. owned a U.N.L. Fellowship. D.E.R. is a member of CONICET. This work was supported by CONICET PIP 2000-02559 and 2005-5370 and UNL-CAI+D 3-23−2006.

Supporting Information Available: Figures showing the *z* diagonal component of the order parameter tensor of SA molecules and the structure factor calculated for the SA molecules and table showing the averaged values of the fraction of dihedrals in the trans conformation of SA molecules. This material is available free of charge via the Internet at http://pubs.acs.org.

References and Notes

(1) McConnell, H. M. In *SPIN LABELING. Theory and Applications*; Berliner, L. J., Ed.; Academic Press: New York, 1976; Chapter 13.

(2) Griffith H.; Jost P. In *SPIN LABELING. Theory and Applications*; Berliner, L. J., Ed.; Academic Press: New York, 1976; Chapter 12.

(3) Risse, T.; Hill, T.; Schmidt, G.; Hamman, H.; Freund, H. J. *J. Phys. Chem. B* **1998**, *102*, 2668−2676.

(4) Risse, T.; Hill, T.; Schmidt, G.; Hamman, H.; Freund, H. J. J. *Chem. Phys.* **1998**, *108*, 8615−8625.

(5) Taylor, M. G.; Smith, I. C. *Biochim. Biophys. Acta* **1983**, *733*, 256−63.

(6) Rivas, M. G.; Gennaro, A. M. *Chem. Phys. Lipids* **2003**, *122*, 165−169.

(7) Cassera, M. B.; Silber, A. M.; Gennaro, A. M. *Biophys. Chem.* **2002**, *99*, 117−127.

(8) Carrer, D. C.; Schreier, S.; Patrito, M.; Maggio, B. *Biophys. J.* **2006**, *90*, 2394−2403.

(9) Rodi, P. M.; Cabeza, M. S.; Gennaro, A. M. *Biophys. Chem.* **2006**, *122*, 114−122.

(10) Hakansson, P.; Westlund, P. O.; Lindahl, E.; Edholm, O. *Phys. Chem. Chem. Phys.* **2001**, *3*, 5311−5319.

(11) Wisniewska, A.; Nishimoto, Y.; Hyde, J. S.; Kusumi, A.; Subczynski, W. K. *Biochim. Biophys. Acta* **1996**, *1278*, 68−72.

(12) Patra, M.; Karttunen, M.; Hyvonen, M. T.; Falck, E.; Vattulainen, I. *J. Phys. Chem. B* **2004**, *108*, 4485−4494.
(13) Hofsass, C.; Lindahl, E.; Edholm, O. *Biophys. J.* **2003**, *84*, 2192−2206.
(14) Falck, E.; Patra, M.; Karttunen, M.; Hyvönen, M. T.; Vattulainen, I. *Biophys. J.* **2004**, *87*, 1076−1091.
(15) Gawrisch, K.; Eldho, N. V.; Polozov, I. V. *Chem. Phys. Lipids* **2002**, *116* (1−2), 135−51.
(16) Ocko, B. M.; Kelley, M. S. *Langmuir* **2002**, *18*, 9810−9815.
(17) Peng, J. B.; Barnes, G. T.; Gentle, I. R. *Adv. Colloid Interface Sci.* **2001**, *91*, 163−219.
(18) Alonso, A.; Meirelles, N. C.; Tabak, M. *Chem. Phys. Lipids* **2000**, *104*, 101−111.
(19) Höltje, M.; Förster, T.; Brandst, B.; Engels, T.; von Rybinski, W.; Höltje, H. *Biochim. Biophys. Acta* **2001**, *1511*, 156−167.
(20) Ulman A. *An introduction to Ultrathin Organic Films From Langmuir-Blodgett to Self-Assembly*; Academic Press: Boston, MA, 1991.
(21) Kaganer, V.; Mohwald, H.; Dutta, P. *Rev. Mod. Phys.* **1999**, *71*, 779−816.
(22) Vogel, A.; Scheidt, H. A.; Huster, D. *Biophys. J.* **2003**, *85*, 1691−1701.
(23) Mouritsen, O. G.; Zuckermann, M. J. *Lipids* **2004**, *39*, 1001−1113.
(24) McMullen, T. P. W.; Lewis, R. N. A. H.; McElhaney, R. N. *Curr. Opin. Colloid Interface Sci.* **2004**, *8*, 459−468.
(25) Ekelung, K.; Sparr, E.; Engblom, J.; Wennerstrom, H.; Engstrom, S. *Langmuir* **1999**, *15*, 6946−6949.
(26) Berger, O.; Edholm, O.; Jahnig, F. *Biophys. J.* **1997**, *72*, 2002−2013.
(27) Ryckaert, J. P.; Bellemans, A. *Faraday Discuss. Chem. Soc.* **1975**, *66*, 95−106.
(28) Berendsen, H. J. C.; Postma, J. P. M.; van Gunsteren, W. F.; Hermans, J. In *Intermolecular Forces*; Pullman, B., Ed.; Interaction Models for Water in Relation to Proteins Hydration; 1981; pp 331−342.
(29) Allen, F. H. *Acta Crystallogr., Sect. B* **2002**, *58*, 380−388.
(30) Bordeaux, D.; Gagnaire, G.; Lajzérowicz, J. *Acta Crystallogr., Sect. C* **1983**, *39*, 466−470.
(31) Bordeaux, D.; Lajzerowicz-Bonneteau, J. *Acta Crystallogr., Sect. B* **1974**, *30*, 2130−2132.
(32) Gleason, W. B. *Acta Crystallogr., Sect. B* **1973**, *29*, 2959−2960.
(33) van Aalten, M. F.; Bywater, R.; Findlay, J. B. C.; Hendlich, M.; Hooft, R. W. W.; Vriend, G. *J. Comput.-Aided Mol. Des.* **1996**, *10*, 255−262.
(34) Schmidt, M. W.; Baldridge, K. K.; Boats, J. A.; Elbert, S. T.; Gordon, M. S.; Jensen, J. H.; Koseki, S.; Matsunaga, N.; Nguyen, K. A.; Su, S.; Windus, T. L.; Dupuis, M.; Montgomery, J. A. *J. Comput. Chem.* **1993**, *14*, 1347−1363.
(35) Breneman, C. M.; Wiberg, K. M. *J. Comput. Chem.* **1990**, *11*, 361−373.
(36) Hess, B.; Bekker, H.; Berendsen, H. J. C.; Fraaije, G. J. E. M. *J. Comput. Chem.* **1997**, *18*, 1463−1472.
(37) Improta, R.; di Matteo, A.; Barone, V. *Theor. Chem. Acc.* **2000**, *104*, 273−279.
(38) Murzyn, K.; Hóg, T.; Blicharski, W.; Dutka, M.; Pyka, J.; Szitula, S.; Froncisz, W. *Proteins* **2006**, *62*, 1088−1100.
(39) Bayly, C.; Cieplak, P.; Cornell, W. D.; Kollman, P. *J. Phys. Chem.* **1993**, *97*, 10269−10280.
(40) Cornell, W. D.; Cieplak, P.; Bayly, C.; Kollman, P. *J. Am. Chem. Soc.* **1993**. *115*, 9620−9631.
(41) Refson, K. *Moldy's user manual*, 2001.
(42) Berendsen, H. J. C.; van der Spoel, D.; van Drunen, R. *Comput. Phys. Commun.* **1995**, *91*, 43−56.
(43) Lindahl, E.; Hess, B.; van der Spoel, D. *J. Mol. Model.* **2001**, *7*, 306−317.
(44) Berendsen, H. J. C.; Postma, J. P. M.; DiNola, A.; Haak, J. R. *J. Chem. Phys.* **1984**, *81*, 3684−3690.
(45) Berendsen, H. J. C. In *Computer Simulations in Material Science*, Meyer, M., Pontikis V., Eds.; Transport properties computed by linear response through weak coupling to a bath; 1991; pp 139−155.
(46) Feller, S. E. *Curr. Opin. Colloid Interface Sci.* **2000**, *5*, 218−224.
(47) Feller, S. E.; Pastor, R. W. *J. Chem. Phys.* **1999**, *111*, 1281−1287.
(48) Lindahl, E.; Edholm, O. *Biophys. J.* **2000**, *79*, 426−433.
(49) Merger, F.; Wood, M. G.; Richardson, S. D.; Zhou, Q. Z.; Elrington, A. R. *J. Am. Chem. Soc.* **1988**, *110*, 6797−6803.
(50) Nagle, J. F.; Tristram-Nagle, S. *Biochim. Biophys. Acta* **2000**, *1469*, 159−195.
(51) Kucerka, N.; Kiselev, M. A.; Balgavý, P. *Eur. Biophys. J.* **2004**, *33*, 328−334.
(52) Lairion, F.; Disalvo, A. E. *Biochim. Biophys. Acta* **2007**, *1768*, 450−456.
(53) Pasenkiewicz-Gierula, M.; Takaoka, Y.; Miyagawa, H.; Kitamura, K.; Kusumi, A. *J. Phys. Chem. A* **1997**, *101*, 3677−3691.
(54) Chapman, D. In *Biomembranes. Physical Aspects*; Shinitzky, M., Ed.; Lipid Phase Transition; Bababon Publishers: Weinheim, Germany, 1993.
(55) Daura, X.; Gademann, K.; Jaun, B.; Seebach, D.; van Gunsteren, W. F.; Mark, A. E. *Angew. Chem., Int. Ed. Engl.* **1999**, *38*, 236−240.
(56) Hautman, J.; Klein, M. L. *J. Chem. Phys.* **1990**, *93*, 7483−7492.
(57) Pake, G. E. *Paramagnetic Resonance*; Benjamin: New York, 1962.
(58) Aittoniemi, J.; Róg, T.; Niemela, P.; Pasienkiewicz-Gierula, M.; Karttunen, M.; Vattulainen, I. *J. Phys. Chem. B* **2006**, *110*, 25562−25564.
(59) Tristram-Nagle, S.; Zhang, R.; Suter, R. M.; Worthington, C. R.; Sun, W. J.; Nagle, J. F. *Biophys. J.* **1993**, *64*, 1097−109.
(60) Subczynski, W. K.; Hyde, J. S.; Kusumi, A. *Proc. Natl. Acad. Sci. U.S.A.* **1989**, *86*, 4474−4478.